A Journal of the Gesellschaft Deutscher Chemiker

Angewandte International Edition

GDCh

Chemie

www.angewandte.org

Accepted Article

Title: Electrocatalytic 5-(hydroxymethyl)furfural oxidation using high surface area nickel boride

Authors: Stefan Barwe, Jonas Weidner, Steffen Cychy, Dulce M Morales, Stefan Dieckhöfer, Dennis Hiltrop, Justus Masa, Martin Muhler, and Wolfgang Schuhmann

To be cited as: *Angew. Chem. Int. Ed.* 10.1002/anie.201806298
Angew. Chem. 10.1002/ange.201806298

Link to VoR: http://dx.doi.org/10.1002/anie.201806298
http://dx.doi.org/10.1002/ange.201806298

WILEY-VCH

10.1002/anie.201806298

WILEY-VCH

COMMUNICATION

Electrocatalytic 5-(hydroxymethyl)furfural oxidation using high surface area nickel boride

Stefan Barwe[#,a], Jonas Weidner[#,a], Steffen Cychy[b], Dulce M. Morales[a], Stefan Dieckhöfer[a], Dennis Hiltrop[b], Justus Masa[a], Martin Muhler[b], Wolfgang Schuhmann*[,a]

Abstract: The electrochemical oxidation of the biorefinery product 5-(hydroxymethyl)furfural (HMF) to 2,5-furandicarboxylic acid (FDCA), an important platform chemical for the polymer industry, receives increasing interest. FDCA-based polymers such as polyethylene 2,5-furandicarboxylate (PEF) are potential sustainable green candidates for replacing polyethylene terephthalate (PET). Here, we report the highly efficient electrocatalytic oxidation of HMF to FDCA using Ni foam modified with high surface area nickel boride (Ni_xB) as electrode. Constant potential electrolysis in combination with high performance liquid chromatography (HPLC) revealed a high faradaic efficiency of close to 100 % towards the production of FDCA with a yield of 98.5 %. *Operando* electrochemistry coupled to attenuated total reflection infrared spectroscopy indicates that HMF is oxidized preferentially via 5-hydroxymethyl-2-furancarboxylic acid rather than 2,5-diformylfuran as intermediate in agreement with HPLC results. This study does not only report a low cost active electrocatalyst material for the electrochemical oxidation of HMF to FDCA, but additionally provides new insight into the reaction pathway.

Upgrading of biorefinery products such as 5-(hydroxymethyl)furfural (HMF) into important industrial feedstock tackles the transition from petroleum-based chemistry towards green and renewable resources. Hydrogenation of HMF leads to the formation of high energy biofuels like 2,5-dimethylfuran (DMF),[1] whereas 2,5-furandicarboxylic acid (FDCA) derived from HMF oxidation was reported to be a “green” platform chemical for the chemical industry with the prospect to replace terephthalic acid as building block for the synthesis of highly valuable polymers.[2,3] FDCA-based polyethylene 2,5-furandicarboxylate (PEF) is considered to be a renewable alternative for the massively used polyethylene terephthalate (PET).[1,2] The thermochemical or electrochemical oxidation of HMF is mostly performed at alkaline conditions to provide the necessary hydroxide ions.[4] Thus, electrocatalytic HMF oxidation can be suitably coupled with the electrocatalytic hydrogen evolution reaction (HER), leading to an additional product of high economic value, thereby increasing the energy efficiency of the electrochemical HER.[5] HMF can be converted to FDCA by either homogeneous or heterogeneous catalysts.[6] However, homogeneous catalysis of HMF conversion mainly suffers from relatively low FDCA yields and poor selectivity. Although an optimised metal bromide-based homogenous catalyst developed already in 1958 allows FDCA yields of 90 %, the separation of FDCA and the recycling of the catalyst remain challenging.[7] On the other hand, heterogeneous catalysts can be separated from the reaction mixture more easily. High costs of the conventionally employed heterogeneous noble metal catalysts such as Pt[8], Au[9], Pd[10] and Ru[11] warrant the effort to replace them with transition metal-based catalysts and to find alternative methods for HMF oxidation. In 1990, Grabowski et al. reported the selective electrochemical oxidation of HMF to FDCA in NaOH (1.0 M) using a $Ni(OH)_2$ electrode. However, the yield was only 71 %.[12] The comparatively low yield despite high selectivity can be explained by the decomposition of HMF in alkaline solutions.[13,14] At high pH values (>13), HMF degrades into humin-type products thereby decreasing the effective HMF concentration, hence leading to lower than expected product yields. However, HMF oxidation at a Pt electrode at lower pH values (pH 10) formed only trace amounts of FDCA.[13] Evidently, a high working pH value therefore facilitates the selective electrochemical oxidation of HMF to FDCA notwithstanding its degradation.[14] Thus, in order to increase the product yield, the development of highly active electrocatalysts is of extreme importance. HMF oxidation using Au, Pd and their alloys supported on carbon black revealed a dependence from catalyst properties, applied potential and oxidation pathway.[15] However, despite noble metal-based electrocatalysts exhibit a low overpotential for HMF oxidation, they only provide low current densities due to surface oxidation and surface blocking. Thus, large electrode surfaces with high catalyst loading are required in order to achieve fast reaction rates.[15] Recently, transition metal-based electrocatalysts, especially compounds or alloys of nickel and cobalt with main-group elements (e.g. P and S) as well as layered double hydroxides (LDHs), were reported to be efficient elecrocatalysts for the selective oxidation of HMF to FDCA achieving high conversion and yield.[14,16] However, recent reports show that NiFe LDHs lack stability during prolonged exposure to highly alkaline electrolyte solutions[17], while transition metal/main group element alloys, e.g phosphides and borides form a highly stable core-shell structure with the initial alloy in the core protected by a metal hydroxide/oxyhydroxide shell.[18,19] We reported ultrathin high surface area nickel boride as highly active bifunctional HER and oxygen evolution reaction (OER) catalyst.[18] Inspired by promising results about HMF oxidation using metal/non-metal alloys, we report high surface area nickel boride (Ni_xB) as electrocatalyst to efficiently and selectively oxidize HMF to the prospective

[a] Dr. S. Barwe, J. Weidner, D. M. Morales, S. Dieckhöfer, Dr. J. Masa and Prof. Dr. W. Schuhmann
Analytical Chemistry – Center for Electrochemical Sciences (CES)
Faculty of Chemistry and Biochemistry, Ruhr-Universität Bochum
Universitätsstrasse 150, 44780 Bochum (Germany)
E-mail: wolfgang.schuhmann@rub.de

[b] S. Cychy, D. Hiltrop and Prof. Dr. M. Muhler
Laboratory of Industrial Chemistry
Faculty of Chemistry and Biochemistry, Ruhr-Universität Bochum
Universitätsstrasse 150, 44780 Bochum (Germany)

# These authors contributed equally to this work

Supporting information for this article is given via a link at the end of the document.

10.1002/anie.201806298

platform chemical FDCA in an electrochemical flow-through reactor coupled with downstream analysis of the products by means of high performance liquid chromatography (HPLC). Additionally, we investigated - to the best of our knowledge for the first time - the preferred reaction pathway by *operando* electrochemistry coupled attenuated total reflection infrared (EC-ATR-IR) spectroscopy.

High surface area Ni_xB was prepared as already reported in detail elsewhere.[18,20] Briefly, Ni_xB was formed by the reduction of nickel chloride by means of sodium borohydride under oxygen-free conditions and subsequent annealing at 300 °C under Ar atmosphere. The product consisted of discrete nanoparticles and very thin sheets that were X-ray amorphous.[18] For an in-depth characterisation of the Ni_xB used in this work, including X-ray photoelectron spectroscopy, X-ray absorption spectroscopy, X-ray diffraction, high resolution transmission electron microscopy, atomic force microscopy and electrochemical water splitting, see Masa et al.[18] This work is intended to solely focus on the electrochemical transformation of HMF into FCDA and its investigation by means of HPLC and *operando* EC-ATR-IR. Electrochemical HMF oxidation over Ni_xB was performed in an electrochemical flow-through reactor (Figure 1) consisting of a Ni_xB-modified Ni foam (NF) and unmodified NF as anode and cathode, respectively (for further information see SI). Both electrode compartments were separated by a PEEK-reinforced anion exchange membrane. A Hg/HgO reference electrode was placed in the anode compartment for potential determination. The anode and cathode compartments were fed with 1 M KOH with and without 10 mM HMF, respectively.

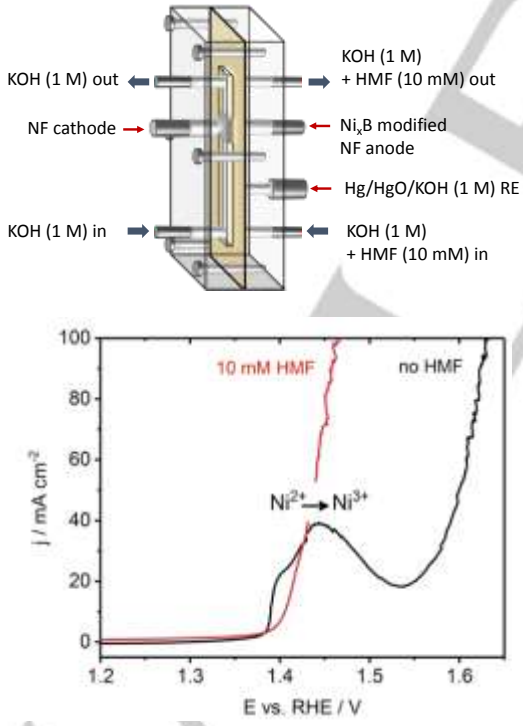

Figure 1. Schematic representation of the electrochemical flow reactor (top). LSV of Ni_xB-modified NF in 1 M KOH in the absence and presence of 10 mM HMF with a scan rate of 2 mV s^{-1} at an electrolyte flow rate of 18 mL min^{-1} (bottom).

SEM images of bare and Ni_xB spray-coated NF show a clear distinction with small Ni_xB particles clearly visible on the latter (Figure S1). The activity of Ni_xB-modified NF towards HMF oxidation was determined by hydrodynamic linear sweep voltammetry (LSV) at an electrolyte (1 M KOH) flow rate of 18 mL min^{-1} (Figure 1). The electrochemical HMF (10 mM) oxidation achieves a high current density of 100 mA cm^{-2} at a potential of 1.45 V vs. RHE, 170 mV lower than the potential necessary to drive the OER at the same current density (Figure 1). In the absence of HMF, Ni^{2+} to Ni^{3+} oxidation is represented by a pronounced pre-OER peak at 1.44 V vs. RHE. There is a discernible shoulder on the cathodic side of the Ni^{2+} to Ni^{3+} oxidation peak, which reveals that the Ni^{2+} to Ni^{3+} peak is a convolution of the oxidation of Ni from Ni_xB and from the NF support (Figure S2). In the presence of HMF (10 mM), the Ni^{2+} to Ni^{3+} oxidation peak was no longer observed. Interestingly, the more cathodic oxidation feature originating from the NF substrate also disappears in the presence of HMF although HMF oxidation starts at slightly more anodic potentials. Similar observations can be made when bare Ni foam is investigated for the electrochemical HMF oxidation (Figure S2), in the presence of HMF, the Ni^{2+} to Ni^{3+} peak is not visible anymore although HMF oxidation starts at more anodic potentials. It can be observed that the currents in the presence of HMF rise slowly prior the potential of the $Ni^{2+/3+}$ oxidation recorded in the absence of HMF (Figure S2b). The absence of the Ni oxidation feature is indeed correlated with the presence of HMF and might be overlaid by it. The formation of the higher oxidation state of the transition metal, in this case Ni^{3+}, is a necessary prerequisite for the electrochemical oxidation of alcohols and aldehydes.[21] The presence of HMF altered the electrochemical response showing an oxidation process at more cathodic potentials as compared to the OER, which is evidently due to electrochemical HMF oxidation. Although the high currents observed by LSV indicate high activity of Ni_xB towards HMF oxidation, however, no conclusion about selectivity, reaction pathway, product distribution and yield can be drawn solely based on this data. Thus, down-stream analysis is necessary in order to elucidate the reaction pathways ultimately leading to the products of electrochemical HMF oxidation. Constant potential electrolysis at a potential with apparently negligible OER (1.45 V vs. RHE) coupled with HPLC at different stages of the electrolysis allowed monitoring HMF oxidation and the nature of the formed products or intermediates. Oxidation of HMF begins with the oxidation of either the carbonyl or the hydroxyl group to form 5-hydroxymethyl-2-furancarboxylic acid (HMFCA) or the dialdehyde 2,5-diformylfuran (DFF), respectively. Thus, the reaction can proceed via two different pathways (Figure 2). Further oxidation of the intermediates HMFCA and DFF leads to the formation of 5-formyl-2-furancarboxylic acid (FFCA) and finally to FDCA. Upon applying a constant potential of 1.45 V vs. RHE the current density instantaneously increased to around 55 mA cm^{-2}. After 2 min, the current density started to decrease, approaching zero after around 35 min (Figure 3a). Correspondingly, the transferred charge showed a steep increase approaching 58.2 C after around 30 min. A charge of 58.2 C for the oxidation of 10 mL 10 mM HMF solution agrees well with the theoretically necessary 6 F mol^{-1} for the complete 6 e^- oxidation of HMF to FDCA, thus pointing to a high faradaic efficiency of HMF oxidation to the desired product FDCA.

10.1002/anie.201806298

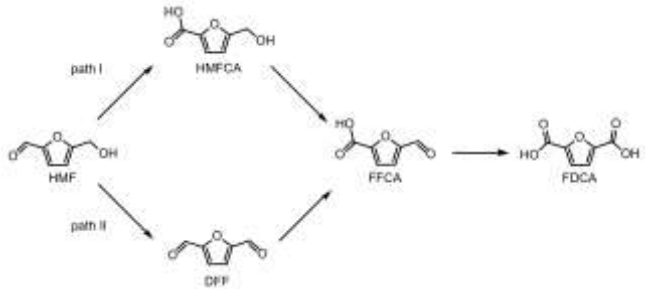

Figure 2. Reaction pathways of HMF oxidation. Path I begins with the aldehyde oxidation forming HMFCA. Path II begins with the oxidation of the alcohol group of HMF leading to the formation of DFF.

HPLC results at different times of the electrolysis qualitatively reveal HMF oxidation to FDCA (Figure 3b, reference chromatograms Figure S3). The signal attributed to HMF at a retention time of 6.92 min continuously decreased while that of FDCA at a retention time of 2.88 min increased with time. The intermediate products HMFCA and FFCA were also detected in traces. Interestingly, DFF as possible intermediate of HMF oxidation was not observed in the chromatograms. Calibration with standard solutions of pure HMF, FDCA and the intermediates allows for quantification of the compounds during electrolysis (Figure S4). After 10 min of electrolysis, 64 % HMF was converted mainly into FDCA and trace amounts of HMFCA and FFCA as intermediates (Figure 3c). Since the intermediate products do not accumulate during the process, fast transformation of HMFCA and FFCA into FDCA is suggested. Full HMF conversion was achieved within 30 min with a high FDCA yield of 98.5 % and a faradaic efficiency of close to 100 % (Figure 3c). The very high yield of 98.5 % emphasises the high activity of Ni_xB towards electrocatalytic HMF oxidation at the applied potential, especially considering a HMF decomposition rate of 10 %/h (for a 10 mM HMF in 1 M KOH solution, see Figure S5). Evidently, using a highly active catalyst for electrochemical HMF oxidation substantially minimizes the extent of the competing chemical degradation of HMF in highly alkaline solution.

Ni_xB modified NF was investigated after electrolysis by means of SEM and X-ray photoelectron spectroscopy (XPS). SEM images after electrochemical HMF oxidation (Figure S6) show an intact catalyst film with no obvious changes in the film appearance as compared with a freshly prepared electrode. Additionally, the freshly prepared catalyst powder, a fresh Ni_xB modified NF and Ni_xB modified NF after electrochemical HMF oxidation were investigated by XPS (Figure S7). A main binding energy of 852.5 eV in the Ni $2p_{3/2}$ spectrum of the freshly prepared Ni_xB powder is in good agreement of metallic Ni and Ni in contact with B as in Ni_2B (Figure S7a).[18] Slight surface oxidation occurring when exposed to air[18] is indicated by the presence of a $Ni(OH)_2$ related peak at binding energies of 855.8 eV (Figure S7a). Similarly, the B 1s core-level spectrum shows signals originating from elemental B/B-Ni and boron-oxo species at binding energies of 187.9 eV and 191.8 eV, respectively (Figure S7b). After spray coating and subsequent HMF electrolysis, the Ni $2p_{3/2}$ core-level spectra reveal an oxidized catalyst surface, with $Ni(OH)_2$, NiO and NiOOH as main components (Figure S7c,e). After spray coating, boron is only present in its oxidized form (B 1s at 192.8 eV) at the catalyst surface (Figure S7d), while it can barely be detected at the surface after electrolysis (Figure S7f). Recently, we investigated Ni_xB and surface oxidation by suspending Ni_xB in a water/ethanol mixture (for spray coating) and applying anodic potentials was similarly observed.[18] The surface oxidation leads to the formation of a core-shell type catalyst with oxidized Ni species ($Ni(OH)_2$, NiO and NiOOH) in the shell and Ni_xB in the core.[18]

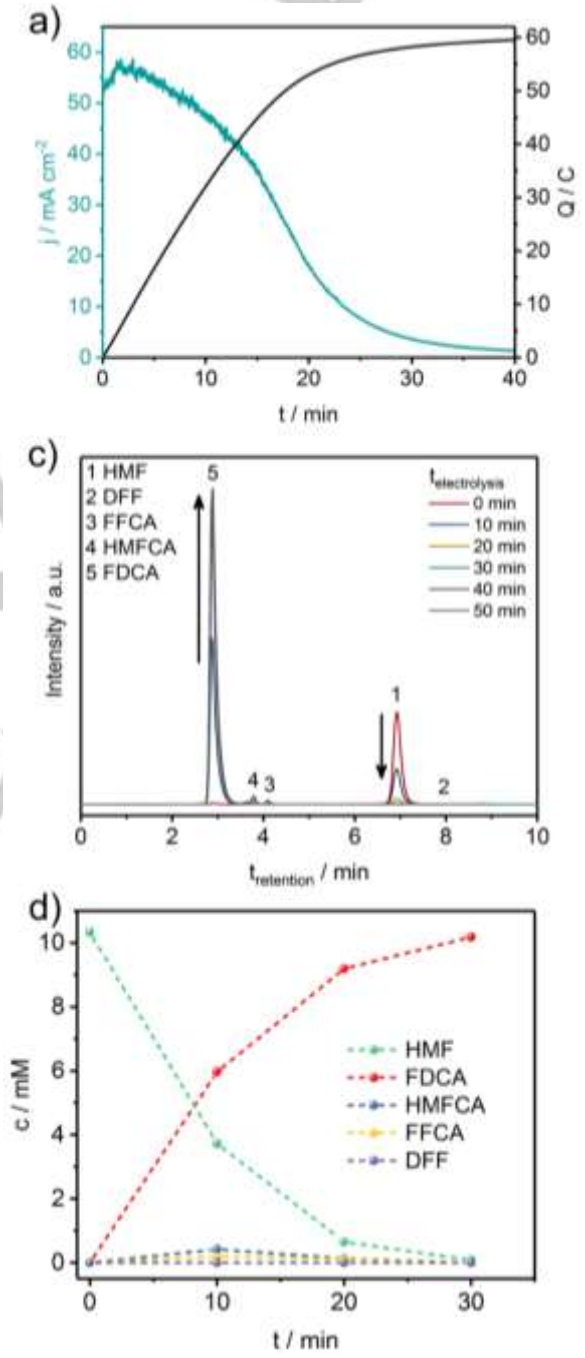

Figure 3. Current-time and charge-time transients during constant potential (1.45 V vs. RHE) electrolysis of a 10 mL solution of 10 mM HMF in 1 M KOH using a Ni_xB modified NF anode in a flow reactor with an electrolyte flow rate of 18 mL min^{-1} (a). HPLC chromatograms taken at various electrolysis times (b). Concentration vs. time plot of HMF, FDCA and the intermediates at various electrolysis times (c).

10.1002/anie.201806298

In order to obtain further insight into the mechanistic details of the electrochemical oxidation of HMF over Ni_xB, *operando* electrochemistry coupled attenuated total reflection infrared (EC-ATR-IR) spectroscopy was employed. A detailed description of the EC-ATR-IR unit and its micrometer-precise positioning of the working electrode above the ATR crystal was recently reported.[22] LSV at EC-ATR-IR conditions reveals a minor current increase at potentials lower than 1.45 V vs. RHE and a steep increase in the current response with increasing potential (Figure S8). The early increase in current cannot unambiguously be assigned to HMF oxidation, since it might overlay with the Ni^{2+} to Ni^{3+} oxidation. Additional discussion of *operando* IR can be found in the supporting information (Figures S9-S12). The assignment of the IR bands and thus the correlation with the different reaction intermediates was based on comparison with reference spectra (Figure S9) of the pure compounds. The representation of the ATR-IR spectra as the logarithm of the reciprocal reflection leads to downwards and upwards pointing bands for consumed and formed species, respectively. IR spectra recorded during a potential step experiment in the potential range from 0.98 V to 1.78 V vs. RHE do not only confirm the oxidation of HMF to FDCA, but also indicate a potential of 1.18 V vs. RHE, at which first IR bands point towards slow HMFCA formation. The bands at wavenumbers of 1386 cm^{-1} and 1351 cm^{-1} and their typical fork-type shape correlate well with the appearance of the HMFCA reference spectrum. At a potential of 1.38 V vs. RHE the reaction is considerably enhanced, leading to more pronounced HMFCA bands at 1355 cm^{-1}, 1388 cm^{-1}, 1529 cm^{-1} and 1569 cm^{-1}, while simultaneously, HMF is consumed as indicated by the downwards pointing bands at 1027 cm^{-1}, 1189 cm^{-1}, 1513 cm^{-1} and 1660 cm^{-1}. The fork-shaped signal at wavenumbers between 1335 cm^{-1} and 1400 cm^{-1} clearly points to HMFCA as the first detectable intermediate at low potentials. Higher potentials led to further HMF depletion and the appearance of characteristic bands for FFCA and FDCA. The bands at 960 cm^{-1}, 975 cm^{-1}, 1276 cm^{-1}, 1407 cm^{-1}, and 1674 cm^{-1} correlate well with the reference spectrum of FFCA. The very intense peak at 1351 cm^{-1} can neither be unambiguously assigned to FFCA nor to FDCA, since both compounds give rise to this band due to the symmetric vibration of their carboxylate groups. However, FDCA formation is indicated by its characteristic band at 1386 cm^{-1}. Complete conversion of HMF to FDCA cannot be achieved in the thin layer cell of the EC-ATR-IR unit due to fast reactant depletion in front of the electrode, slow mass transport solely governed by diffusion and short reaction times. Therefore, the recorded spectra at higher potentials remain convolutions of formed FFCA and FDCA. Nevertheless, complete HMF oxidation into FDCA in the flow reactor was proved by HPLC. The possible formation of DFF and its fast oxidation, and thus its absence in the IR spectra and HPLC chromatograms, cannot be ruled out completely. Additionally, the close similarity of the IR spectra of HMF and DFF complicates their clear differentiation. However, IR spectroscopy of DFF and HMFCA in KOH (0.1 M) without applying any potential reveals base-catalysed oxidation of DFF to FFCA, while HMFCA did not react without an applied potential (Figures S11&S12). Consequently, although DFF signals might not be clearly assignable, if HMF oxidation would preferentially follow the reaction pathway II depicted in Figure 2, FFCA-related signals must appear in the IR spectra recorded at low potentials and without the appearance of HMFCA related bands. The absence of DFF- and FFCA-related bands at low applied potentials is in good agreement with the HPLC data and strengthens our conclusion that electrocatalytic HMF oxidation on Ni_xB preferentially follows the HMFCA pathway.

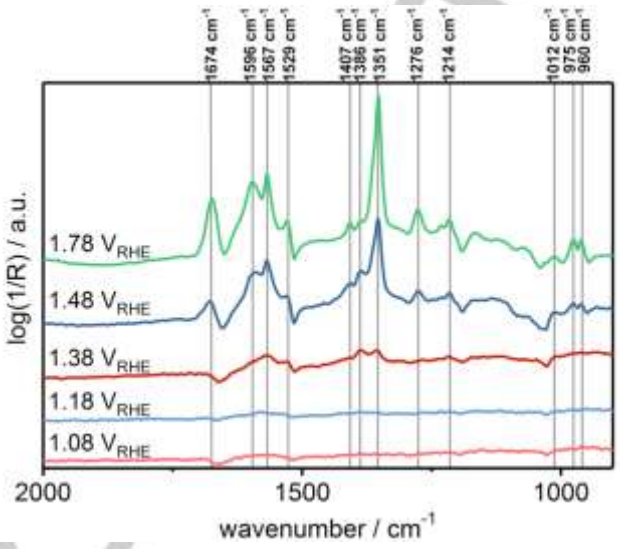

Figure 4. *Operando* ATR-FTIR spectra at various applied potentials between 0.98 V vs. RHE and 1.78 V vs. RHE after 20 minutes of applied potential. Potential steps were 100 mV.

In conclusion, we present the selective and efficient electrocatalytic oxidation of the biorefinery product HMF to FDCA over Ni_xB-modified NF in an electrochemical flow-through reactor. A very high FDCA yield of 98.5 % was achieved at a faradaic efficiency of 100 %. Investigation of the product formation and intermediate formation by means of HPLC and *operando* EC-ATR-IR complementary revealed HMF oxidation via the HMFCA intermediate rather than the DFF pathway. Thus, Ni_xB appears is identified as promising catalyst for electrocatalytic HMF oxidation, an important reaction for upgrading biorefinary products thus paving the way into “green chemistry”.

Acknowledgements

This work was supported by the Deutsche Forschungsgemeinschaft (DFG) in the framework of the cluster of excellence RESOLV (EXC 1069) and the CRC/TRR 247 (project A2). The authors are grateful to Mrs. Sandra Schmidt for the SEM images and to Dr. Thomas Erichsen and Dr. Dirk Wolters for their help with the HPLC measurements. D. M. Morales acknowledges the financial support from Deutscher Akademischer Austauschdienst (DAAD) and from Consejo Nacional de Ciencia y Tecnología (CONACyT).

Keywords: electrocatalysis • HMF oxidation • nickel boride • operando electrochemistry ATR-IR • electrosynthesis

References

[1] Y. Kwon, K. J. P. Schouten, van der Waal, Jan C., E. de Jong, M. T. M. Koper, *ACS Catal.* **2016**, *6*, 6704–6717.

[2] J. J. Bozell, G. R. Petersen, *Green Chem.* **2010**, *12*, 539–554.

[3] a) Eerhart, A. J. J. E., A. P. C. Faaij, M. K. Patel, *Energy Environ. Sci.* **2012**, *5*, 6407–6422; b) R.-J. van Putten, van der Waal, Jan C, E. de Jong, C. B. Rasrendra, H. J. Heeres, J. G. de Vries, *Chem. Rev.* **2013**, *113*, 1499–1597.

[4] R. Latsuzbaia, R. Bisselink, A. Anastasopol, H. van der Meer, R. van Heck, M. S. Yagüe, M. Zijlstra, M. Roelands, M. Crockatt, E. Goetheer et al., *J. Appl. Electrochem.* **2018**, *38*, 4901 (1-16).

[5] H. G. Cha, K.-S. Choi, *Nat. Chem.* **2015**, *7*, 328–333.

[6] a) T. S. Hansen, I. Sádaba, E. J. García-Suárez, A. Riisager, *Appl. Catal. A-Gen.* **2013**, *456*, 44–50; b) B. Saha, S. Dutta, M. M. Abu-Omar, *Catal. Sci. Technol.* **2012**, *2*, 79–81.

[7] X. Zuo, P. Venkitasubramanian, D. H. Busch, B. Subramaniam, *ACS Sustain. Chem. Eng.* **2016**, *4*, 3659–3668.

[8] a) H. Ait Rass, N. Essayem, M. Besson, *ChemSusChem* **2015**, *8*, 1206–1217; b) H. Ait Rass, N. Essayem, M. Besson, *Green Chem.* **2013**, *15*, 2240–2251; c) S. Siankevich, G. Savoglidis, Z. Fei, G. Laurenczy, D. T. Alexander, N. Yan, P. J. Dyson, *J. Catal.* **2014**, *315*, 67–74; d) Z. Miao, T. Wu, J. Li, T. Yi, Y. Zhang, X. Yang, *RSC Adv.* **2015**, *5*, 19823–19829; e) S. E. Davis, L. R. Houk, E. C. Tamargo, A. K. Datye, R. J. Davis, *Catal. Today* **2011**, *160*, 55–60.

[9] a) Z. Miao, Y. Zhang, X. Pan, T. Wu, B. Zhang, J. Li, T. Yi, Z. Zhang, X. Yang, *Catal. Sci. Technol.* **2015**, *5*, 1314–1322; b) J. Cai, H. Ma, J. Zhang, Q. Song, Z. Du, Y. Huang, J. Xu, *Chem. Eur. J.* **2013**, *19*, 14215–14223; c) A. Villa, M. Schiavoni, S. Campisi, G. M. Veith, L. Prati, *ChemSusChem* **2013**, *6*, 609–612; d) N. K. Gupta, S. Nishimura, A. Takagaki, K. Ebitani, *Green Chem.* **2011**, *13*, 824–827.

[10] a) B. Liu, Y. Ren, Z. Zhang, *Green Chem.* **2015**, *17*, 1610–1617; b) N. Mei, B. Liu, J. Zheng, K. Lv, D. Tang, Z. Zhang, *Catal. Sci. Technol.* **2015**, *5*, 3194–3202; c) Z. Zhang, J. Zhen, B. Liu, K. Lv, K. Deng, *Green Chem.* **2015**, *17*, 1308–1317.

[11] Z. Zhang, K. Deng, *ACS Catal.* **2015**, *5*, 6529–6544.

[12] G. Grabowski, J. Lewkowski, R. Skowroński, *Electrochim. Acta* **1991**, *36*, 1995.

[13] K. R. Vuyyuru, P. Strasser, *Catal. Today* **2012**, *195*, 144–154.

[14] D.-H. Nam, B. J. Taitt, K.-S. Choi, *ACS Catal.* **2018**, *8*, 1197–1206.

[15] D. J. Chadderdon, Le Xin, J. Qi, Y. Qiu, P. Krishna, K. L. More, W. Li, *Green Chem.* **2014**, *16*, 3778–3786.

[16] a) B. You, X. Liu, N. Jiang, Y. Sun, *J. Am. Chem. Soc.* **2016**, *6*, 6704–6717; b) N. Jiang, B. You, R. Boonstra, I. M. Terrero Rodriguez, Y. Sun, *ACS Energy Lett.* **2016**, *1*, 386–390; c) B. You, N. Jiang, X. Liu, Y. Sun, *Angew. Chem. Int. Ed.* **2016**, *55*, 9913–9917; d) W.-J. Liu, L. Dang, Z. Xu, H.-Q. Yu, S. Jin, G. W. Huber, *ACS Catal.* **2018**, *8*, 5533–5541.

[17] C. Andronescu, S. Seisel, P. Wilde, S. Barwe, J. Masa, Y.-T. Chen, E. Ventosa, W. Schuhmann, *Chem. Eur. J.* **2018**.

[18] J. Masa, I. Sinev, H. Mistry, E. Ventosa, M. de La Mata, J. Arbiol, M. Muhler, B. Roldan Cuenya, W. Schuhmann, *Adv. Energy Mater.* **2017**, *78*, 1700381.

[19] a) J. Masa, S. Barwe, C. Andronescu, I. Sinev, A. Ruff, K. Jayaramulu, K. Elumeeva, B. Konkena, B. Roldan Cuenya, W. Schuhmann, *ACS Energy Lett.* **2016**, 1192–1198; b) J. Masa, P. Weide, D. Peeters, I. Sinev, W. Xia, Z. Sun, C. Somsen, M. Muhler, W. Schuhmann, *Adv. Energy Mater.* **2016**, *6*, 1502313-1 – 1502313-10.

[20] B. Ganem, J. O. Osby, *Chem. Rev.* **1986**, *86*, 763–780.

[21] a) M. Fleischmann, K. Korinek, D. Pletcher, *J. Chem. Soc., Perkin Trans. 2* **1972**, 1396–1403; b) A. Kowal, S. N. Port, R. J. Nichols, *Catal. Today* **1997**, *38*, 483–492.

[22] D. Hiltrop, J. Masa, A. J. R. Botz, A. Lindner, W. Schuhmann, M. Muhler, *Anal. Chem.* **2017**, *89*, 4367–4372.

10.1002/anie.201806298

WILEY-VCH

Entry for the Table of Contents (Please choose one layout)

Layout 1:

COMMUNICATION

The selective and efficient electrocatalytic oxidation of the biorefinery product HMF to the prospective platform chemical FDCA over nickel boride (Ni_xB) modified nickel foam in an electrochemical flow through reactor exhibits a very high FDCA yield of 98.5 % at a faradaic efficiency of 100 %. Ni_xB appears to be a very promising catalyst for electrochemical HMF oxidation.

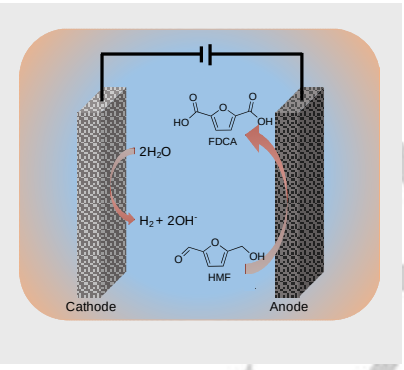

Stefan Barwe, Jonas Weidner, Steffen Cychy, Dulce M. Morales, Stefan Dieckhöfer, Dennis Hiltrop, Justus Masa, Martin Muhler, Wolfgang Schuhmann

Page No. – Page No.

Electrocatalytic 5-(hydroxymethyl)furfural oxidation using high surface area nickel boride